ACS APPLIED POLYMER MATERIALS

pubs.acs.org/acsapm

Article

# Biopolypropylene-Based Wood Plastic Composites Reinforced with Mango Peel Flour and Compatibilized with an Environmentally Friendly Copolymer from Itaconic Acid

Jaume Gomez-Caturla,* Rafael Balart, Juan Ivorra-Martinez, Daniel Garcia-Garcia, Franco Dominici, Debora Puglia, and Luigi Torre

Cite This: *ACS Appl. Polym. Mater.* 2022, 4, 4398−4410

Read Online

ACCESS | Metrics & More | Article Recommendations | Supporting Information

**ABSTRACT:** This work reports on the successful development of biopolypropylene/mango peel flour (bioPP/MPF) composites using extrusion and injection molding processes. The compatibility between bioPP and MPF is improved through the use of PP-*g*-IA (3 phr) as a compatibilizer (which is prepared by reactive extrusion REX) and dicumyl peroxide (DCP) (1 phr) as a cross-linker. The mechanical, morphological, thermal, thermomechanical, chemical, colorimetric, water absorption, and flowability properties are characterized and analyzed. The results show that MPF (30 wt %) compatibilized with PP-*g*-IA and DCP increased the stiffness of bioPP in terms of Young's modulus values. Elongation at break also shows very promising results, with a maximum value of almost 30% for the bioPP/MPF/PP-*g*-IA/DCP sample. PP-*g*-IA and DCP seem to exert a synergetic effect. Thermal stability is also improved as a result of these additives, as well as crystallinity, which is increased due to an heterogeneous nucleation phenomenon, enhanced by a higher dispersion of MPF particles in the matrix. Moreover, the excellent mechanical results are verified in FESEM images, where a very narrow gap between the MPF particles and the bioPP matrix is appreciated.

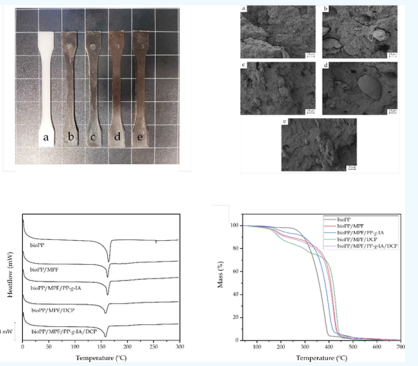

**KEYWORDS:** *polymer composites, biopolymers, reinforcements, mango peel flour, compatibilization*

## 1. INTRODUCTION

In the recent years, society is becoming more concerned about the environmental issues provoked by the excessive use of petrochemical plastics, such as the increase in greenhouse gas emission related to the production process of those materials. This problem has led both industry and the scientific community to look for more environmentally friendly alternatives. One of this alternatives is the development and use of fully or partially biobased polymeric materials obtained from natural resources that could substitute conventional petrochemical polymers.[1,2] In this field, wood plastic composites (WPCs) have become an interesting solution as these are the combination of a base polymer (or biopolymer) and a wood-like (or more generally, a lignocellulosic) reinforcement/filler.[3,4] These fillers reduce the cost of the materials and at the same time improve some of their physical and chemical properties, leading to multifunctional materials.[5,6] At first, only wood flour and sawdust were used as organic fillers, but lately, plant-derived lignocellulosic fillers coming from different industries have been gaining importance,[7] such as almond shell flour,[8] hemp fiber,[9] or pineapple leaves,[10] among others.

Among all the polymers, polypropylene (PP) has gained quite a lot of popularity, being a semicrystalline thermoplastic with a very good balance between resistant and ductile mechanical properties and chemical resistance.[11] Thus, considering that biopolymers possess the same properties as that of their petrochemical counterparts,[12] biopolypropylene (bioPP) is a very promising option to be considered as a biopolymeric matrix in WPCs. The production of bioPP has not been explored as much as the production of biopolyethylene (bioPE), but it can be obtained from methanol, further processed to obtain the propylene monomer and then polymerized to obtain bioPP.[13] However, one of the main drawbacks of using natural organic fillers with nonpolar polymers, such as polyolefins, is the polarity of the fillers, associated with the presence of lignocellulosic (lignin, cellulose, and hemicellulose) constituents in their structure (with hydroxyl groups),[14] which makes them highly hydrophilic, while the biopolymer matrix is marked by high hydrophobicity. This fact directly leads to a poor mechanical

Received: March 3, 2022
Accepted: April 27, 2022
Published: May 5, 2022

response in these polymer/filler systems, related to a lack of interfacial adhesion and affinity between them.

In order to improve the compatibility between the filler and the surrounding matrix, several studies have been carried out based either on the surface modification of the filler or on the use of a compatibilizing agent, which increases the hydrophilicity of the base polymer.[15] On the one hand, some methods such as benzoylation, silanization, or acetylation involve surface modification of the lignocellulosic particles by blocking the hydroxyl groups.[16] On the other hand, a wide range of copolymers have been used to increase the affinity between the filler and the matrix. Some of the most used copolymers are polyethylene or PP subjected to grafting with maleic anhydride (PP-*g*-MA and PP-*g*-MA, respectively), which use the maleic anhydride group to increase the polarity of PE and PP and act as a chemical bridge between natural fillers and the polymeric chains.[17] More recently, itaconic acid (IA), which can be obtained from renewable resources (i.e., from citric acid), has been proposed as an environmentally friendly grafting monomer, acting as a polar functionalization agent for nonpolar polymers, such as PP. Pesetskii et al.[18] modified PP by reactive extrusion (REX) with dicumyl peroxide (DCP) in order to obtain the corresponding grafted copolymer PP-*g*-IA with interesting compatibilization properties. Moncada et al.[19] reported the superior compatibilizing effect of PP-*g*-IA in a PP/clay nanocomposite when compared to conventional PP-*g*-MA. Kim et al.[20] also reported the effectiveness of PP-*g*-IA as a compatibilizer in PP/EVOH blends, avoiding phase separation. These compatibilizers usually solve the compatibility problem between lignocellulosic fillers and polymer matrices, but the overall properties obtained are not so remarkable.

REX allows polymers to react during the extrusion process through the formation of free radicals, whose formation can be catalyzed by organic peroxides.[21] In this context, DCP has been widely reported as an excellent free-radical initiator, which facilitates the reaction of polymers with functional groups, which is especially useful in the case of low-miscibility physical blends, such as polylactide/poly(butylene adipate-*co*-terephthalate) (PLA/PBAT)[22] and poly(3-hydroxybutyrate), and poly($\varepsilon$-caprolactone) blends,[23] among others. Not only has DCP been used in polymer blends but also in polymer−fiber composites, as it is the case of the work reported by Ahmad and Luyt,[24] which shows a clear improvement in the interactions between PE and sisal fiber for a concentration of DCP of 1 phr (parts by weight of DCP per 100 weight parts of the base polymer) during REX.

Mango (*Mangifera indica* L.) is one of the most popular fruits in the planet, as it is the fifth largest major fruit crop when it comes to world production.[25] There are several varieties that are quite marketable because of their flavor and taste. The main wastes from this fruit are the exocarp (peel), the endocarp (pit or stone), and the kernel or seed. Mango peel has been reported to be a lignocellulosic compound with a high polyphenol content,[26] while the mango kernel is mainly composed of starch, protein, and fatty acids;[27] on the other hand, the endocarp (pit or stone) is rich in cellulose, hemicelluloses, and lignin.[28] The circular economy concept makes mango one of the most interesting wastes to take benefit from, one of its applications being the development of WPCs with additional functional properties and at a more competitive cost. Moreover, mango wastes have not been greatly reported in the literature for producing WPCs.

There are hardly any investigations regarding the use of mango wastes as fillers for green composites. Hence, the main aim of this work is to develop WPCs with partially biobased PP (bioPP) as the polymer matrix and mango peel flour (MPF) as a novel reinforcing component, in order to reduce the cost of the polymer and, at the same time, improve its properties. The leading obstacle and challenge in this study is the difference in polarity and hydrophilicity between the filler and the matrix, as bioPP is a highly nonpolar polymer, while MPF, being a lignocellulosic filler, is a highly polar component. To overcome this issue, an environmentally friendly grafted copolymer of PP and IA (PP-*g*-IA) is obtained by REX with DCP as a free-radical initiator. Several formulations have been developed by extrusion (REX in the case of DCP) and injection moulding to obtain composites of bioPP with MPF with improved properties by using PP-*g*-IA and DCP, both individually and in combination. Then, the properties of these composites have been evaluated by means of mechanical, morphological, thermal, thermomechanical, colorimetric, chemical, and wettability characterization.

## 2. EXPERIMENTAL SECTION/METHODS

**2.1. Materials.** Biobased PP was supplied by NaturePlast (Caen, France).

Mangoes of the Palmer-Kent variety were purchased from the local market in Alcoy, Spain. The mangoes were peeled, and the peels were first dried at 50 °C for 48 h in a dehumidifying stove (MCP Vacuum Casting System, Lubeck, Germany) to remove any residual moisture. The peels were then crushed and milled in a ZM 200 centrifugal mill from Retsch (Düsseldorf, Germany) at a speed of 8000 rpm and finally sieved with a 250 $\mu$m mesh filter, obtaining the MPF. MPF particles show a rough surface with an average length of 50 $\mu$m and an average width of 15 $\mu$m, as it can be observed in Figure S1 from the Supporting Information.

DCP 98% was supplied by Sigma-Aldrich (product code: 1003031352), and IA 99+% was supplied by Acros Organics (product code: 122810010).

**2.2. Grafting of PP-*g*-IA.** The IA grafting process was performed following the methodology described by Pesetskii et al.,[18] using DCP as the initiator. BioPP, IA, and DCP were dried at 40 °C for 48 h in a dehumidifying dryer MDEO to remove any residual moisture prior to processing. Then, 1 wt % of IA was blended with bioPP and 0.2 wt % DCP, according to the study carried out by Pesetskii et al.[18] The grafting was conducted using a twin-screw extruder from Construcciones Mecánicas Dupra, S.L. (Alicante, Spain). This extruder has a 25 mm diameter with a length-to-diameter ratio (L/D) of 24. The residence time of the compounds in the extruder was approximately 4 min. The temperature profile from the hopper to the extrusion die was 175−195−195−195 °C. After the extrusion, PP-*g*-IA was pelletized using an air-knife unit.

**2.3. Preparation of BioPP/MPF Composites.** BioPP, MPF, PP-*g*-IA, and DCP were initially dried at 40 °C for 48 h in a dehumidifying dryer MDEO to remove the residual moisture. Then, each formulation was mixed according to Table 1. The corresponding formulations were compounded in a twin-screw extruder from Construcciones Mecánicas Dupra, S.L. (Alicante, Spain). This extruder has a 25 mm diameter with a length-to-diameter ratio (L/D) of 24. The extrusion process was carried out at a rate of 22 rpm, using the following temperature profile (from the hopper to the die): 150−155−160−165 °C. The compounded materials were pelletized using an air-knife unit. In all cases, the residence time was approximately 1 min. Table 1 shows the compositions of the formulations developed in this work.

To shape the pellets into standard samples, a Meteor 270/75 injection moulding machine from Mateu & Solé (Barcelona, Spain) was used. The temperature profile in the injection moulding unit was 155 °C (hopper), 160, 165, and 170 °C (injection nozzle). A



https://doi.org/10.1021/acsapm.2c00373
ACS Appl. Polym. Mater. 2022, 4, 4398−4410

**Table 1. Summary of Compositions According to the Weight Content (wt %) of BioPP/MPF and Different Compatibilizers and Additives**

| code | BioPP (wt %) | MPF (wt %) | PP-*g*-IA (phr)[a] | DCP (phr) |
|---|---|---|---|---|
| bioPP | 100 | 0 | 0 | 0 |
| bioPP/MPF | 70 | 30 | 0 | 0 |
| bioPP/MPF/PP-*g*-IA | 70 | 30 | 3 | 0 |
| bioPP/MPF/DCP | 70 | 30 | 0 | 1 |
| bioPP/MPF/PP-*g*-IA/DCP | 70 | 30 | 3 | 1 |

[a]phr stands for the weight part of PP-*g*-IA or DCP per 100 weight parts of the base bioPP/MPF composite.

clamping force of 75 tons was applied, while the cavity filling and cooling times were set to 1 and 10 s, respectively. Standard samples for mechanical and thermal characterization with an average thickness of 4 mm were obtained.

**2.4. Characterization of BioPP/MPF Blends.** *2.4.1. Grafting Efficiency.* Grafting efficiency (ratio of the grafted IA related to its total quantity added to the polymer) was measured by infrared spectroscopy according to the method used by Pesetskii et al.[29] Films of 30−40 $\mu$m thickness were molded from the pellets of PP-*g*-IA at 145 °C. Then, the films were immersed in ethanol at 70 °C in order to extract the ungrafted IA. Grafting efficiency was estimated from the variation in the absorbance of the films at 1720 $cm^{-1}$, which corresponds to the carbonyl groups. The absorbance of the films was measured at different times from the immersion of the films in ethanol (0, 1, 2, 4, 6, 8, 22, 24, and 27 h). The grafting efficiency was determined using eq 1

$$\text{grafting efficiency} = \frac{D_\tau}{D_0} 100\ [\text{wt \%}] \tag{1}$$

where $D_\tau$ and $D_0$ stand for the optical densities related to the thickness of the film once all the ungrafted IA has been extracted and at the initial time before immersion in ethanol, respectively.

*2.4.2. Mechanical Characterization.* The tensile properties of bioPP/MPF composites were determined using an universal testing machine ELIB 50 from S.A.E. Ibertest (Madrid, Spain), as recommended by ISO 527-1:2012. A load cell of 5 kN was used while the cross-head speed was set to 5 mm/min. Shore hardness was measured in a 676 D durometer from J. Bot Instruments (Barcelona, Spain), using the D-scale, on rectangular samples with dimensions 80 × 10 × 4 $mm^3$, according to ISO 868:2003. The impact strength was also studied on injection-molded rectangular samples with dimensions of 80 × 10 × 4 $mm^3$ in a Charpy pendulum (1 J) from Metrotec S.A. (San Sebastián, Spain) on notched samples (V-notch type with a radius of 0.25 mm), following the specifications of ISO 179-1:2010. All mechanical tests were performed at room temperature, and at least six samples of each material were tested, and the corresponding tensile parameters were averaged.

*2.4.3. Morphology Characterization.* The morphology of fractured samples from Charpy tests, obtained from the impact tests, was studied by field emission scanning electron microscopy (FESEM) in a ZEISS ULTRA 55 microscope from Oxford Instruments (Abingdon, United Kingdom). Before placing the samples in the vacuum chamber, they were sputtered with a gold−palladium alloy in an EMITECH sputter coating SC7620 model from Quorum Technologies Ltd. (East Sussex, UK). The FESEM system was operated at an acceleration voltage of 2 kV.

*2.4.4. Thermal Analysis.* The most relevant thermal transitions of bioPP/MPF composites were obtained by differential scanning calorimetry (DSC) in a Mettler-Toledo 821 calorimeter (Schwerzenbach, Switzerland). Samples with an average weight of 6−7 mg were subjected to a thermal program divided into three stages: a first heating from −50 to 200 °C, followed by cooling to 0 °C, and a second heating to 300 °C. Both the heating and cooling rates were set to 10 °C/min. All tests were run in a nitrogen atmosphere with a flow rate of 66 mL/min using standard sealed aluminum crucibles with a capacity of 40 $\mu$L.

$$X_c = \left[\frac{\Delta H_m}{\Delta H_m^0 \cdot (1 - w)}\right] \cdot 100 \tag{2}$$

where $\Delta H_m^0$ = 198 J/g is the theoretical enthalpy of a 100% crystalline PP sample;[30] the term $1 - w$ corresponds to the PP weight fraction in the blend; and $\Delta H_m$ is the measured melting enthalpy.

The thermal degradation of the bioPP/MPF composites was assessed by thermogravimetric analysis (TGA). TGA tests were performed in a LINSEIS TGA 1000 (Selb, Germany) system. Samples with a weight of 15−17 mg were placed in 70 $\mu$L alumina crucibles and subjected to a dynamic heating program from 40 to 700 °C at a heating rate of 10 °C/min in nitrogen atmosphere. The first derivative thermogravimetric (DTG) curves were also determined. All tests were carried out at least three times in order to obtain reliable results.

*2.4.5. Dynamical−Mechanical Thermal Characterization.* Dynamical−mechanical thermal analysis (DMTA) was carried out in a DMA1 dynamic analyzer from Mettler-Toledo (Schwerzenbach, Switzerland), working in single cantilever flexural conditions. Rectangular samples with dimensions of 20 × 6 × 2.7 $mm^3$ were subjected to a dynamic temperature sweep from −150 to 100 °C at a constant heating rate of 2 °C/min. The selected frequency was 1 Hz, and the maximum flexural deformation or cantilever deflection was set to 10 $\mu$m.

*2.4.6. Water Absorption Test.* The water absorption capacity of the bioPP/MPF composites was evaluated by the water uptake method. Rectangular samples with dimensions 80 × 10 × 4 $mm^3$ were first weighed in a balance and then placed inside a beaker filled with distilled water, all of them wrapped with tiny pieces of metal grids so that they could sink. After that, the weight of all samples was measured at intervals of several hours the first day and then measured each week for a total period of 14 weeks in order to evaluate the amount of absorbed water. In every measurement, the moisture on the surface of the samples was removed with a tissue paper.

*2.4.7. Infrared Spectroscopy.* Chemical characterization of the bioPP/MPF composites was carried out by attenuated total reflection−Fourier transform infrared spectroscopy (ATR−FTIR). The spectra were recorded using a Bruker S.A. Vector 22 (Madrid, Spain) instrument coupled to a PIKE MIRacle single-reflection diamond ATR accessory (Madison, Wisconsin, USA). Data were collected as the average of 10 scans between 4000 and 500 $cm^{-1}$ with a spectral resolution of 2 $cm^{-1}$.

*2.4.8. Melt Flow Index.* A melt flow indexer extrusion plastometer from Metrotec (Lezo, Spain) with a cutoff mechanism was used for melt flow index (MFI) determination. The load mass was set at 2.16 kg, and the temperature was established at 190 °C. Approximately 20 g of each sample was put into the indexer, and after 2 min of heating, the load was charged, and the material started to flow. Intervals of 30 s, after which the cutoff mechanism was activated, were set to take samples of each material and calculate their mass. Five tests were carried out for each blend.

## 3. RESULTS AND DISCUSSION

**3.1. Grafting Efficiency of PP-*g*-IA.** Figure 1 shows the variation of absorbance in the 1720 $cm^{-1}$ band through 27 h of extraction in ethanol solution at 70 °C for PP-*g*-IA. The absorbance presented is related to the thickness of the film used in the test. Absorbance drastically decreases in the first hour of extraction and then starts to stabilize until at 22 h it becomes constant at a value of 1.87. This reduction in absorbance is ascribed to the removal of the ungrafted IA in the film, which is released into the ethanol solution, with the true grafted IA only remaining in the PP-*g*-IA copolymer. A very similar extraction profile was observed by Pesetskii et al.[29] when studying the grafting efficiency of IA in the LDPE-*g*-IA copolymer. Using eq 1, the grafting efficiency of PP-*g*-IA was


https://doi.org/10.1021/acsapm.2c00373
ACS Appl. Polym. Mater. 2022, 4, 4398−4410

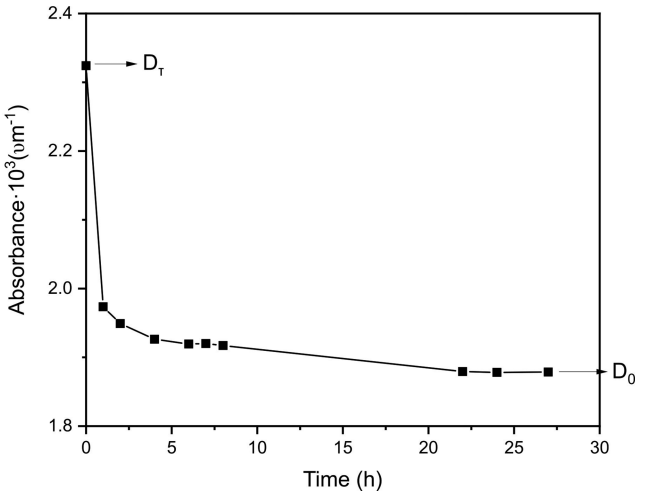


**Figure 1.** Variation of the optical density of the carbonyl group absorption bands (1720 $cm^{-1}$) with extraction time in ethanol.

calculated, giving a value of 82.12 ± 1.83%. This proves that the grafting was successfully carried out, with most of the IA having reacted with bioPP in the REX process. Pesetskii et al.[29] observed a very similar IA grafting efficiency of approximately 85% for a concentration of DCP of 0.2 wt % in the REX process, which is the same proportion used in this study. Considering that REX is a process easily applied in industrial scale, this fact in combination with the high grafting efficiency obtained makes PP-*g*-IA a compatibilizer that would be easily produced not only at laboratory level but also at industrial level. Moreover, as IA is obtained from biosourced citric acid, which is widely available at a relatively low cost, grafting with IA can be a cost-effective process, compared to traditional grafting with maleic anhydride.

**3.2. Mechanical Properties.** Table 2 summarizes the results concerning the mechanical properties of bioPP/MPF composites with DCP and PP-*g*-IA.

It can be seen that neat bioPP showed a tensile modulus ($E$) of 1936 MPa, a maximum tensile strength of 17.71 MPa, and an elongation at break of 38.96%. These values are in accordance with the results reported by Zhou et al.,[11] who reported a value for $E$ modulus of 1890 MPa. These values show that bioPP is a ductile material but with greater stiffness than bioPE.[1] The addition of MPF in the biopolymer matrix clearly reduces all mechanical properties. The tensile modulus and strength are reduced down to 1758 and 11.64 MPa, respectively, while elongation at break is reduced down to 15.98%, which is a reduction of more than 50% in relation to neat bioPP. This reduction could be ascribed to the lack of interaction between MPF and bioPP, as MPF is a lignocellulosic compound rich in polyphenols[26] and, hence, with a high number of hydroxyl groups, while bioPP is a nonpolar biopolymer, with no functional groups to interact with MPF.[31] This fact leads to a poor interaction of the MPF particles with the bioPP matrix, thus decreasing its mechanical cohesive properties, mainly the tensile strength and the elongation at break. A similar trend was observed by Yadav and Yusoh[32] in PP composites with wood flour, which decreased its tensile strength by 15%. The addition of PP-*g*-IA in the bioPP/MPF composite increases all of its tensile properties, reaching a tensile modulus of 2237 MPa, a tensile strength of 13.51 MPa, and an elongation at break of 18.86%. These results suggest that PP-*g*-IA effectively acts as a compatibilizer, increasing the affinity and interaction of the MPF particles with the surrounding bioPP matrix, even surpassing the tensile modulus ($E$) of neat bioPP. A similar behavior was observed by Poletto[33] in PP/wood flour composites. Nevertheless, the most important thing is that the addition of PP-*g*-IA leads to an increase in both cohesive properties, the tensile strength and the elongation at break, which is clear evidence of the effectiveness of the PP-*g*-IA compatibilizer in comparison with the most commonly used PP-*g*-MA compatibilizer. Morandim-Giannetti et al.[34] studied the effect of PP-*g*-MA on PP/coir fiber composites, showing that PP-*g*-MA increased the tensile strength but drastically reduced the elongation at break (1.3%). This fact clearly demonstrates that PP-*g*-IA proves to be a superior compatibilizer in PP/lignocellulosic composites. The addition of DCP during REX of bioPP/MPF composites increases all the mechanical properties even more than PP-*g*-IA, leading to a tensile modulus of 2280 MPa, a tensile strength of 14.17 MPa, and a clear interesting improved elongation at break of 28.13%. This increase in the mechanical response represents the cross-linking effect that DCP exerts over the polymer chains with the lignocellulosic filler, thus giving support to the compatibilization between both components. DCP promotes free-radical formation on both bioPP polymer chains and the different compounds in MPF, thus allowing a wide variety of reactions between them, improving the interaction between bioPP and MPF. Some studies have reported the ability of DCP to induce free-radical reaction between polymers, such as low-density polyethylene (LDPE), and cellulose fibers.[35] Considering that MPF has cellulose in its chemical composition, the obtained results are consistent with previous studies, therefore demonstrating the strengthening effect of DCP over the blend. Finally, the bioPP/MPF/PP-*g*-IA/DCP composite offers the best tensile mechanical properties of all developed composites, even besting neat bioPP in terms of tensile modulus, changing from 1936 to 2349 MPa, which is an increase of 21.33% in relation to neat bioPP. Tensile strength and elongation at break state at 14.39 MPa and 29.69%, respectively, are not so far from the neat bioPP values. These results suggest some synergetic effect between DCP and PP-*g*-IA, which achieve better mechanical properties than when used

**Table 2. Summary of the Mechanical Properties of the Injection-Molded Samples of bioPP/MPF Composites[a]**

| code | $E$ (MPa) | $\sigma_{max}$ (MPa) | $\varepsilon_b$ (%) | Shore $D$ hardness | impact strength (kJ/$m^2$) |
|---|---|---|---|---|---|
| bioPP | 1936 ± 211 | 17.71 ± 0.77 | 38.96 ± 1.26 | 62.4 ± 0.6 | 9.95 ± 0.59 |
| bioPP/MPF | 1758 ± 105 | 11.64 ± 0.30 | 15.98 ± 1.63 | 61.7 ± 0.6 | 2.83 ± 0.33 |
| bioPP/MPF/PP-*g*-IA | 2237 ± 149 | 13.51 ± 0.13 | 18.86 ± 1.3 | 61.3 ± 0.4 | 2.80 ± 0.19 |
| bioPP/MPF/DCP | 2280 ± 191 | 14.17 ± 0.23 | 28.13 ± 1.67 | 63.6 ± 1.4 | 3.63 ± 0.43 |
| bioPP/MPF/PP-*g*-IA/DCP | 2349 ± 170 | 14.39 ± 0.25 | 29.69 ± 1.63 | 63.6 ± 0.8 | 3.78 ± 0.19 |

[a]Tensile modulus ($E$), maximum tensile strength ($\sigma_{max}$), elongation at break ($\varepsilon_b$), Shore D hardness, and impact (Charpy) strength.



https://doi.org/10.1021/acsapm.2c00373
ACS Appl. Polym. Mater. 2022, 4, 4398−4410

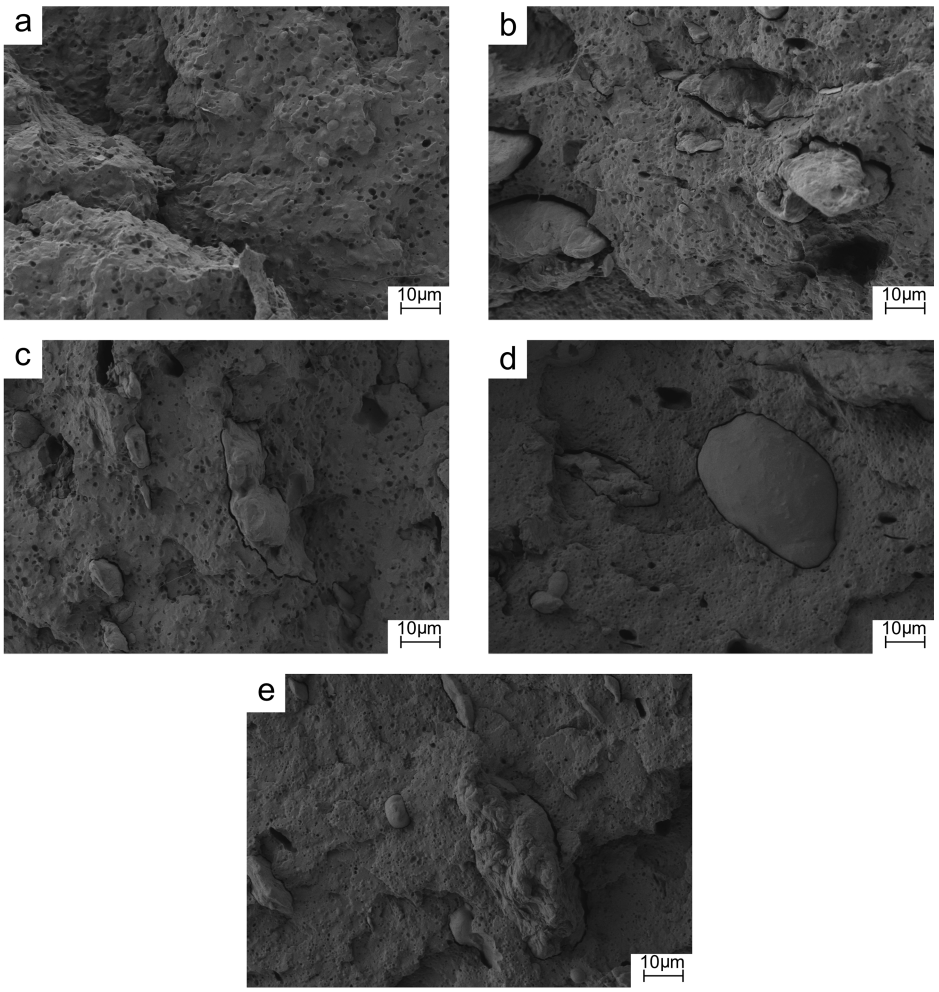


**Figure 2.** FESEM images at 1000× of the fractured surfaces of: (a) bioPP; (b) bioPP/MPF; (c) bioPP/MPF/PP-*g*-IA; (d) bioPP/MPF/DCP; and (e) bioPP/MPF/PP-*g*-IA/DCP.

separately. It can be concluded that the interaction of MPF with bioPP polymer chains is enhanced by the combined effect of both DCP and PP-*g*-IA.

Regarding Shore D hardness, all the bioPP-based composites tested in this study showed values in the 61−64 range. Neat bioPP presented a hardness of 62.4, which is slightly lower than that reported by Caraschi and Leão[36] for neat PP. The addition of MPF seems to slightly decrease the hardness of bioPP, although it is not a significant reduction. This agrees with the tensile properties reported previously, as a reduction in the stiffness of the material is responsible for lowered resistance to deformation. The addition of PP-*g*-IA did not significantly vary the hardness of the base composite. On the other hand, composites obtained by REX with DCP showed a slight increase in hardness up to 63.6 for both of them. This slight increase in hardness also remarks the improved interactions between bioPP and MPF. Compatibilization also prevents the aggregate formation and improves the overall mechanical response of bioPP/MPF composites. Finally, impact strength was highly affected by the addition of MPF, PP-*g*-IA, and DCP. Neat bioPP exhibited an impact strength of 9.95 kJ/m$^2$ on notched samples, which is indicative of a ductile material, as previously observed by elongation at break. The addition of MPF into the bioPP matrix significantly reduced the impact strength down to 2.83 kJ/m$^2$. It is important to bear in mind that the impact strength is also a mechanical property related to cohesion. This large decrease could be ascribed to the embrittlement of the material as a result of MPF aggregation that would lead to the stress concentration phenomenon.[37] The addition of PP-*g*-IA copolymer into the blend does not improve the impact strength, with values around 2.8 kJ/m$^2$. On the other hand, REX with DCP does increase the impact strength up to 3.63 and 3.78 kJ/m$^2$ for bioPP/MPF/DCP and bioPP/MPF/PP-*g*-IA/DCP, respectively, which also reflects some synergistic effect by using PP-*g*-IA and DCP during REX compounding. This increase in relation to uncompatibilized bioPP/MPF could be related to the effect of DCP, which enhances the adhesion and dispersion of MPF in the biopolymer matrix and, probably, provides a better particle−matrix interface interaction. Sari et al.[38] reported how the impact strength of pandanwangi fiber-reinforced polyethylene composites increased with the content of DCP during REX.

All in all, these results point out to the fact that PP-*g*-IA and DCP act as excellent compatibilizers for MPF and bioPP by REX, highly increasing the overall mechanical response of the bioPP/MPF blend and even surpassing neat bioPP in terms of tensile modulus.

**3.3. Morphology of bioPP/MPF Composites.** The mechanical properties of these composites are strongly related to their internal structure. Figure 2 shows the FESEM images at 1000× magnification of the fractured surface of impact test



https://doi.org/10.1021/acsapm.2c00373
ACS Appl. Polym. Mater. 2022, 4, 4398−4410

Table 3. Melting Temperature ($T_m$), Melting Enthalpy ($\Delta H_m$), and Degree of Crystallinity ($X_c$) of BioPP/MPF Composites with Different Compatibilization Strategies, Obtained by DSC[a]

| | DSC parameters | | | TGA parameters | | |
|---|---|---|---|---|---|---|
| samples | $T_m$ (°C) | $\Delta H_m$ (J/g) | $X_C$ (%) | $T5\%$ (°C) | $T_{deg}$ (°C) | residual weight (%) |
| bioPP | 164.0 ± 2.1 | 84.4 ± 1.1 | 42.6 ± 0.4 | 272.8 ± 0.8 | 382.3 ± 2.4 | 0.3 ± 0.1 |
| bioPP/MPF | 161.9 ± 1.9 | 69.4 ± 0.6 | 50.0 ± 0.5 | 182.4 ± 1.1 | 417.9 ± 1.3 | 0.1 ± 0.1 |
| bioPP/MPF/PP-*g*-IA | 162.1 ± 2.0 | 78.0 ± 0.9 | 58.0 ± 0.5 | 208.4 ± 1.4 | 398.9 ± 1.8 | 0.1 ± 0.2 |
| bioPP/MPF/DCP | 158.1 ± 1.8 | 67.9 ± 1.5 | 49.5 ± 0.3 | 168.4 ± 0.5 | 429.4 ± 2.2 | 0.2 ± 0.2 |
| bioPP/MPF/PP-*g*-IA/DCP | 157.9 ± 2.4 | 69.8 ± 1.3 | 52.4 ± 0.4 | 177.4 ± 1.2 | 417.4 ± 1.0 | 0.1 ± 0.1 |

[a]Main thermal degradation parameters of bioPP/MPF composites with different compatibilization strategies in terms of the onset degradation temperature at a mass loss of 5 wt % ($T_{5\%}$), maximum degradation rate (peak) temperature ($T_{deg}$), and residual mass at 700 °C.

samples from uncompatibilized and compatibilized bioPP/MPF composites. Figure 2a corresponds to neat bioPP, and it shows the typical cavernous surface with high roughness, which is ascribed to the plastic deformation of the polymer, indicating the ductile behavior.[39] When MPF was added to the polymer matrix, the lignocellulosic particles presented poor adhesion in the case of the uncompatibilized bioPP/MPF composite (Figure 2b), which is clearly demonstrated by the huge gap between the MPF particles and the surrounding bioPP matrix. This is ascribed to the low interaction between these two components as a result of bioPP being nonpolar and MPF being highly polar. Nagmouchi et al.[40] observed the same phenomenon when studying the compatibility of olive stone flour lignocellulosic particles with a PP matrix, observing gaps between the fillers and the matrix. This corroborates the poor mechanical properties reported in Section 3.1. The addition of PP-*g*-IA into the bioPP/MPF composite (Figure 2c) clearly improves the material cohesion between the MPF lignocellulosic particles and the bioPP matrix, which can be deduced from the reduction in the gap between both components. Toro et al.[41] reported the improvement in compatibility and the resistance mechanical properties of PP with mineral fillers by compatibilizing with PP-*g*-IA. This is ascribed to the dual functionality of PP-*g*-IA. On the one hand, PP chains can interact with the bioPP matrix, while the polar IA groups can interact with the hydroxyl groups in MPF.[42] REX with DCP (Figure 2d) exhibited an even better compatibility between MPF particles and the surrounding bioPP, as MPF particles are quite embedded into the polymer matrix and present a very narrow gap between them, increasing their mechanical performance. This fact is indicative of the reactive compatibilization that DCP exerts over lignocellulosic particles and the bioPP matrix during REX, as it has been mentioned in the Mechanical Properties section. Finally, Figure 2e shows the FESEM image for the bioPP/MPF/PP-*g*-IA/DCP composite. In this case, the particle−matrix gap seems almost inexistent, which again points out to the fact that the combination of PP-*g*-IA and DCP during REX provides a synergistic compatibilization effect.

All in all, the observed morphologies are in total agreement with the mechanical properties mentioned above, demonstrating that PP-*g*-IA and DCP act as a high-performance compatibilizing system that can overcome the lack of compatibility between the nonpolar bioPP matrix and the dispersed polar MPF particles.

**3.4. Thermal Properties of BioPP/MPF Blends.** Table 3 lists the main thermal parameters corresponding to the DSC second heating cycle from 0 to 300 °C of the studied samples (melting temperature, $T_m$; melting enthalpy, $\Delta H_m$; and the degree of crystallinity, $X_c$). The DSC thermograms can be observed in Figure S2 from Supporting Information. Only the melting temperature can be observed in the temperature range presented here, due to the glass-transition temperature of bioPP being very low (−50 to 10 °C).[43] This transition will be further studied by DMTA analysis. Neat bioPP shows a melting temperature of 164 °C and a degree of crystallinity ($X_c$) of 42.6%. These values are quite similar to the values reported by Shafigullin et al.[30] and typical of PP. The incorporation of MPF into the polymer matrix slightly reduces the melting point down to 161.9 °C, which is ascribed to the intrinsic low thermal stability of the lignocellulosic filler. On the other hand, crystallinity increases up to 50.0% because MPF particles can induce heterogeneous nucleation and promote the crystallization process.[44] With the addition of PP-*g*-IA, the melting temperature slightly increases related to the previous sample, which could be ascribed to the dilution effect toward MPF, as PP-*g*-IA, despite being less thermally stable than bioPP, is more thermally stable than the lignocellulosic particles.[45] The degree of crystallinity also increases up to 58.0%. This could be related to the positive compatibilization of the MPF particles with bioPP thanks to PP-*g*-IA, which improves the particle dispersion all over the matrix, enhancing the heterogeneous nucleation phenomenon. The use of REX with DCP during the compounding of bioPP/MPF composites leads to a decrease in the melting temperature down to 158.1 °C. This effect was also observed by Ahmad and Luyt,[24] who attributed this phenomenon to a decrease in the size of the crystallites and thinner lamella. The degree of crystallinity remained very similar to that of bioPP/MPF, so it can be inferred that REX with DCP only affects the size and shape of the crystals, but the total amount remains almost unaltered. This phenomenon was also observed by Ahmad and Luyt.[24] Finally, the composite compatibilized with the combination of DCP and PP-*g*-IA by REX presents a similar melting temperature compared to the previous sample and a degree of crystallinity of 50.2%, which is the second highest crystallinity degree of all composited ions developed this work. This could be ascribed to the combined compatibilizing effect of PP-*g*-IA and DCP during REX.

Table 3 also lists the main quantitative parameters regarding the thermal degradation behavior of the bioPP/MPF composites. The thermogravimetric (TGA) curves and their first derivatives (DTG) are shown in Figure S3 from Supporting Information. First, bioPP showed the typical single-stage degradation profile of a polyolefin, with an onset degradation temperature (measured at 5 wt % mass loss, $T_{5\%}$) of 272.8 °C while the maximum degradation rate temperature ($T_{deg}$) is located at 382.3 °C. After the degradation process, the residual mass was 0.3 wt %. Essabir et al.[46] reported a similar degradation profile for PP in a study related to the addition of



https://doi.org/10.1021/acsapm.2c00373
ACS Appl. Polym. Mater. 2022, 4, 4398−4410

Table 4. Dynamic−Mechanical Properties of bioPP/MPF Composites with Different Compatibilization Strategies, at Different Temperatures

| parts | $E'$ (MPa) at −100 °C | $E'$ (MPa) at −25 °C | $E'$ (MPa) at 80 °C | $\beta$-relaxation$_{PP}$ (°C)[a] | $\alpha$-relaxation $(T_g)_{PP}$ (°C)[a] |
|---|---|---|---|---|---|
| bioPP | 2318 ± 45 | 1674 ± 21 | 277 ± 7 | −44.9 ± 1.3 | 14.2 ± 1.3 |
| bioPP/MPF | 2563 ± 33 | 1862 ± 27 | 239 ± 9 | −49.0 ± 2.2 | 11.9 ± 2.2 |
| bioPP/MPF/PP-*g*-IA | 2575 ± 28 | 1976 ± 25 | 254 ± 5 | −48.9 ± 2.1 | 18.4 ± 2.1 |
| bioPP/MPF/DCP | 2341 ± 32 | 1774 ± 30 | 210 ± 7 | −49.3 ± 1.7 | 21.7 ± 1.7 |
| bioPP/MPF/PP-*g*-IA/DCP | 2544 ± 40 | 1939 ± 27 | 201 ± 8 | −52.8 ± 1.5 | 15.8 ± 1.5 |

[a] $T_g$ has been measured using the tan $\delta$ peak maximum criterion.

nut-shells of argan particles into a PP polymer matrix. Totally in contrast, the addition of MPF into the bioPP matrix provokes the degradation to occur in three main stages, ascribed to the lignocellulosic nature of the MPF. The first stage in the range 280−340 °C is related to the thermal depolymerization of hemicellulose and pectin. The second one which comprises the temperature range of 340−448 °C corresponds to the degradation of cellulose contained in the MPF particles, and the last one, in the range 448−500 °C, is associated with the progressive degradation of lignin.[46] This degradation profile is observed in all the samples with MPF. In this case, the onset degradation temperature is 182.4 °C, and the maximum degradation rate temperature is 417.9 °C. Interestingly, the composite with bioPP and MPF starts to degrade more rapidly than bioPP but then presents more thermal stability than bioPP and delays the maximum degradation peak by 30 °C. This is because hemicellulose and pectin are poorer in terms of thermal stability than bioPP, while cellulose and lignin possess a higher thermal stability than the polyolefin.[47] When PP-*g*-IA is added into the bioPP/MPF composite, the onset degradation temperature moves up to 208.4 °C, and the degradation temperature goes down to 398.9 °C in relation to the bioPP/MPF composite. These results suggest that PP-*g*-IA slightly reduced the thermal stability of the base bioPP/MPF composite in the final temperature range, which corroborates the results observed by DSC. A similar behavior was observed by Kim et al.[48] in PP/PP-*g*-IA composites with different contents of PP-*g*-IA from 1 to 10 wt %. However, this composite shows greater thermal stability than neat bioPP, with the maximum degradation peak located at 398.9 °C. This result is in accordance with the increase in crystallinity observed by DSC. Comparing PP-*g*-IA with other studies that use PP-*g*-MA instead, the compatibilizer used herein improves the thermal stability at the first stages of degradation, which is the opposite to what was observed by Morandim-Giannetti et al.,[34] whose study showed that PP-*g*-MA reduced the initial degradation temperature of PP/coir fiber composites with 30 wt % of lignocellulosic filler. Similarly, REX with DCP reduces the thermal stability in the first stages of the degradation profile, with $T_{5\%}$ of 168.4 °C. Nonetheless, it delays the most prominent degradation stage up to 429.4 °C. This observation perfectly matches the results obtained by DSC, where the crystallinity of bioPP was increased due to REX with DCP. The combination of PP-*g*-IA and DCP during REX of bioPP/MPF composites gives similar results in comparison to the bioPP/MPF sample. Nonetheless, they improve the overall thermal stability of the composite in almost all the temperature ranges.

**3.5. Dynamic−Mechanical Behavior of BioPP/MPF Composites.** The thermomechanical properties of bioPP/MPF composites were studied by DMTA in the temperature range from −150 to 100 °C. Table 4 lists the main thermomechanical parameters extracted from Figure S4 (Supporting Information), which shows the evolution of the storage modulus $E'$ (Figure S4a) and the dynamic damping factor tan $\delta$ (Figure S4b). Regarding neat bioPP, an initial decrease of the storage modulus can be seen until −60 °C approximately. Then, a more pronounced decrease occurs until 0 °C. Both decreases will be explained in the next paragraph. BioPP exhibits a storage modulus of 2318, 1674, and 277 MPa at −100, −25, and 80 °C, respectively. This decrease in storage modulus is provoked by a softening of the polymer matrix. García-García et al. observed a similar thermomechanical profile for neat PP.[49] The addition of MPF increases the stiffness of the material up to 2563 and 1862 MPa at −100 and −25 °C, respectively. This is due to the presence of a rigid filler that induces mechanical restraint, which reduces the mobility of the polymer chains of bioPP.[49] The addition of PP-*g*-IA increases even more the stiffness of the composite, which is ascribed to the positive compatibilizing effect of the PP-*g*-IA copolymer, demonstrating the improvement in mechanical properties shown in the Mechanical Properties section. DCP increases the rigidity of the materials in almost all the temperature ranges, showing a value of 1774 MPa in comparison with 1674 MPa of neat bioPP at −25 °C. Mishra and Luyt[50] observed how REX with DCP increased the storage modulus of LDPE−nanosilica composites. Finally, the combination of PP-*g*-IA and DCP during REX offers similar values to the bioPP/MPF/PP-*g*-IA sample.

The dynamic damping factor tan $\delta$ allows to determine the different relaxations that occur in the polymer matrix along all the temperature ranges. As it has been aforementioned, two main relaxation peaks are observed for neat bioPP, a less intensive $\beta$-relaxation, which appears at −44.9 °C, and an $\alpha$-relaxation, which is shown at 14.2 °C. The former is related to the mobility devitrification of $-CH_2-$ groups in the main chain, while the latter is ascribed to the glass-transition temperature of the polymer, according to the study of Krivoguz et al.[51] The addition of MPF decreases both relaxation temperatures down to −49 and 11.9 °C, respectively. This is probably due to an inefficient dispersion of the MPF particles in the polymer matrix, which does not allow a positive restriction of chain mobility.[49] On the contrary, the incorporation of PP-*g*-IA and REX with DCP provides a slight increase in the glass-transition temperature. The addition of the PP-*g*-IA copolymer leads to a $T_g$ of 18.4 °C, which is mainly ascribed to the compatibilizing effect of the copolymer. Thus, it allows MPF particles to correctly disperse all over the polymer matrix, increasing the filler−matrix interface interactions and restricting the chain mobility. REX with DCP further increases the glass-transition temperature up to 21.7 °C due to the cross-linking effect DCP can provide, while the combination of PP-*g*-IA and DCP during REX also delays the glass-transition temperature by 15.8 °C in comparison with uncompatibilized bioPP/MPF,


https://doi.org/10.1021/acsapm.2c00373
ACS Appl. Polym. Mater. 2022, 4, 4398−4410

Table 5. Contact Angles ($\theta_w$) of Different bioPP/MPF Composites with Different Compatibilization Strategies at Several Times of Exposure to Distilled Water: 0, 5, 10, 15, 20, and 30 min

| code | time | | | | | |
|---|---|---|---|---|---|---|
| | 0 min | 5 min | 10 min | 15 min | 20 min | 30 min |
| BioPP | 88.4 ± 2.3° | 82.6 ± 3.1° | 79.8 ± 1.5° | 75.5 ± 2.2° | 74.3 ± 2.0° | 65.2 ± 1.6° |
| bioPP/MPF | 79.4 ± 2.1° | 75.1 ± 2.2° | 69.6 ± 1.6° | 65.4 ± 1.2° | 62.8 ± 1.7° | 53.7 ± 1.1° |
| bioPP/MPF/PP-*g*-IA | 91.1 ± 2.9° | 88.2 ± 2.6° | 85.6 ± 3.0° | 80.4 ± 2.2° | 77.0 ± 1.3° | 72.2 ± 1.4° |
| bioPP/MPF/DCP | 81.2 ± 2.2° | 77.9 ± 1.9° | 75.5 ± 1.5° | 74.2 ± 2.4° | 71.9 ± 1.8° | 71.5 ± 2.3° |
| bioPP/MPF/PP-*g*-IA/DCP | 89.5 ± 2.3° | 86.6 ± 3.2° | 83.8 ± 1.8° | 79.4 ± 2.8° | 78.4 ± 4.1° | 76.3 ± 2.9° |

thus making the material more rigid. In general, the improvement in stiffness of all bioPP/MPF composites could be also related to the increase in crystallinity observed by DSC analysis.

**3.6. Wetting Properties and Water Absorption of BioPP/MPF Composites.** One of the main drawbacks of WPCs is their tendency to absorb water, as they contain a high proportion of hydrophilic fillers. Contact angle measurements of a distilled water drop at different times (from 0 to 30 min) have been carried out in order to evaluate the wetting properties of the developed composites. Table 5 summarizes the water contact angle values at 0, 5, 10, 15, 20, and 30 min for uncompatibilized and compatibilized bioPP/MPF composites. At the initial time, all samples are quite hydrophobic, as their contact angles are around 90° and are far superior to the hydrophilic threshold, according to Vogler, which is 65°.[52] These results were expected, as the base material, bioPP, is a highly nonpolar polymer, all its bonds being formed by carbon and hydrogen (C−H). This nonpolarity is what makes bioPP maintain a high contact angle over time, varying its contact angle from 88.4° at 0 min to 65.2° at 30 min. When adding MPF to the bioPP matrix, the contact angle suffered quite a decrease at the initial time, going down to 79.4°, rapidly diminishing to 53.7° at 30 min. This decrease is ascribed to the polarity of the MPF particles, which have a high content in cellulose, hemicellulose, lignin, and other phenolic compounds,[53] all of them having hydrophilic hydroxyl groups. These groups possess a great affinity toward water, a polar solvent, thus increasing its absorption and decreasing the contact angle. This effect is clearly seen in Figure S5 from Supporting Information, which shows how the distilled water drop flattens over time for the uncompatibilized bioPP/MPF composite. Compatibilization with the PP-*g*-IA copolymer seems to increase the hydrophobicity of the blend, maintaining the contact angle from 91.1 to 72.2° at 30 min. Although PP-*g*-IA should decrease the water contact angle due to the polar structure of IA (a carboxylic acid), this high hydrophobicity could be ascribed to a certain esterification reaction between hydroxyl groups in MPF and IA, forming esters that somehow decrease the polarity of MPF particles,[54] which is quite interesting from a practical point of view. The compatibilization by REX with DCP does not increase remarkably the water contact angle all over the time range in comparison to the uncompatibilized bioPP/MPF composite. This could be ascribed to the ability of DCP to increase the polarity in these composites as a consequence of the reaction products obtained from the decomposition of DCP in the extruder, favoring radical formation, which could lead to cross-linking and branching, as it was observed by Rojas-Lema et al.[21] Nonetheless, it gets a contact angle of 71.5 at 30 min, which is quite higher than that of bioPP/MPF. Finally, the bioPP/MPF/PP-*g*-IA/DCP composite exhibits intermediate values between the composite compatibilized with the PP-*g*-IA copolymer and the composite obtained by REX with DCP, although the effect of PP-*g*-IA seems to prevail.

All in all, these results interestingly suggest that the addition of PP-*g*-IA and DCP during compounding by REX can solve the problem of hydrophilicity when adding natural organic particles into nonpolar matrices (bioPP), even increasing its hydrophobicity up to a certain point. Therefore, this could lead to interesting applications, such as decking floors with water isolation properties, making them easier to be cleaned.

In addition to contact angle measurements, Figure 3 shows the water absorption profile of all the developed composites

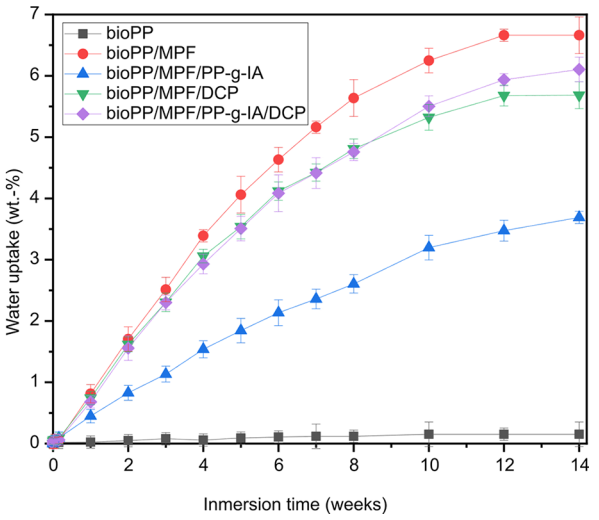


**Figure 3.** Water uptake of uncompatibilized and compatibilized bioPP/MPF composites.

after a long immersion time into distilled water (14 weeks). First, it can be seen how neat bioPP did not absorb barely any water, presenting an asymptotic value of approximately 0.15 wt % of water absorption in relation to its initial mass. This poor water absorption is ascribed to its nonpolar nature, as it has been aforementioned, which makes bioPP to have low affinity for water (a polar solvent). A similar water absorption profile was observed by García-García et al.[49] for neat PP. The addition of MPF increases water absorption up to an asymptotic value of 6.7 wt %. This is mainly ascribed to hydrogen-bond formation between water molecules and hydroxyl groups present in cellulose and hemicellulose in MPF.[55] This fact makes MPF very affine toward water and thus allows the composite to absorb large amounts of water. On the contrary, bioPP/MPF composites compatibilized with PP-*g*-IA reduces water absorption in the whole time range down to approximately 3.7 wt % after 14 weeks of immersion. This is probably due to the fact that PP-*g*-IA can react with the



https://doi.org/10.1021/acsapm.2c00373
ACS Appl. Polym. Mater. 2022, 4, 4398−4410

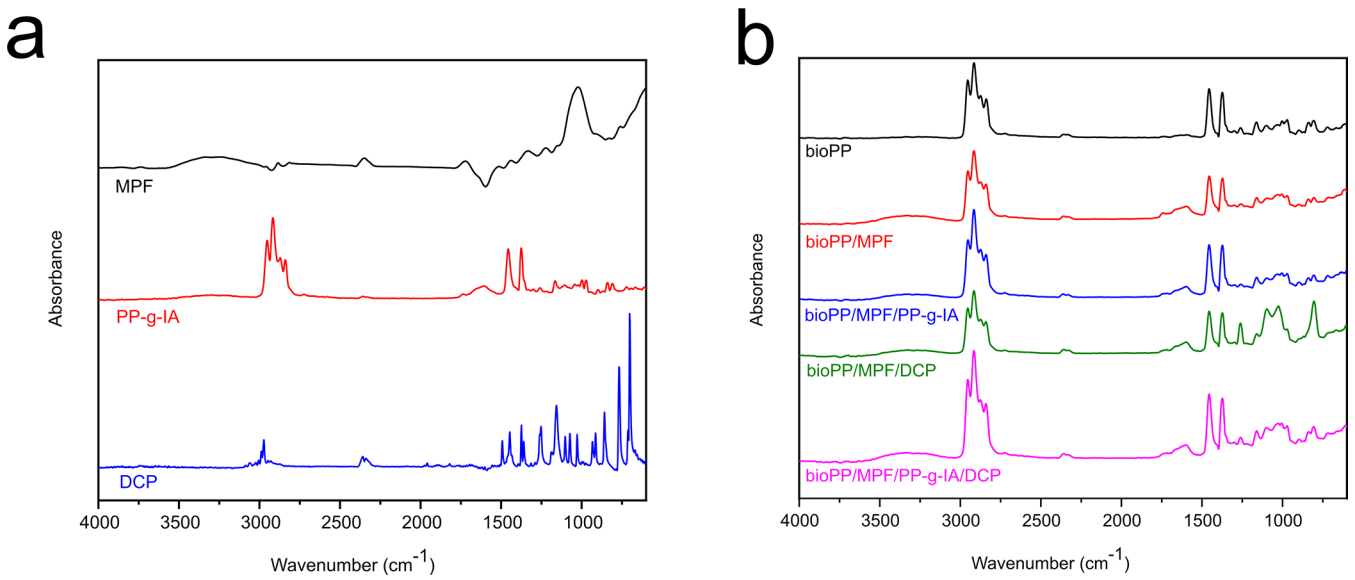


**Figure 4.** FTIR spectra of MPF, PP-*g*-IA, DCP, and uncompatibilized and compatibilized bioPP/MPF composites in the wavenumber range 4000−500 $cm^{-1}$.

hydroxyl groups in MPF, reducing the total amount of free hydroxyl groups in the composite that can interact with water, thus reducing water absorption. García-García et al.[49] observed a very similar effect by the addition of PP-*g*-MA into a PP matrix with spent coffee ground (SCG) particles. On the other hand, REX with DCP does not reduce water absorption remarkably, reaching an asymptotic value of 5.7 wt % water absorption after 14 weeks of immersion in water. This could be ascribed to the fact that the presence of DCP did not result in a great formation of free radicals during REX, thus not impeding the contact between water molecules and cellulose-based compounds in MPF.[56] Finally, the bioPP/MPF composite compatibilized by REX with both DCP and PP-*g*-IA presents a water absorption curve very similar to that of the previous sample, exhibiting an asymptotic value of 6.1 wt % of water absorption at 14 weeks of water immersion. This implies that, somehow, DCP inhibits the ability of PP-*g*-IA to reduce water absorption to a great extent, which could be ascribed to the fact that PP-*g*-IA reacts at a higher degree with bioPP rather than with MPF in this case, as a result of the cross-linking effect of DCP.

These results show that bioPP/MPF composites have great water absorption capabilities. Nonetheless, PP-*g*-IA is able to reduce water absorption down to half the water absorption of the bioPP/MPF composite, which is an interesting property that could prove to be useful in applications where less interaction with water is needed, such as the production of floors, roofs, or windows.

**3.7. Infrared Spectroscopy.** FTIR technique is very useful to analyze the chemical interactions on composites developed in this study. Figure 4a shows the infrared spectra of MPF, PP-*g*-IA, and DCP, while Figure 4b shows the spectra of uncompatibilized and compatibilized bioPP/MPF composites from 4000 to 500 $cm^{-1}$.

First, MPF presents a very typical spectrum of a lignocellulosic filler, with a very characteristic band at 3340 $cm^{-1}$, ascribed to the O−H stretching vibration and hydrogen bonding of hydroxyl groups present in cellulose, hemicellulose, pectin, and lignin. Then, another little peak at 2920 $cm^{-1}$ is related to the C−H stretching vibration in CH and $CH_2$ in cellulose and hemicellulose.[57] The peak at 1730 $cm^{-1}$ is attributed to the carbonyl C═O stretching vibration of carboxylic acid in lignin or ester groups in hemicellulose. The absorption band at 1450 $cm^{-1}$ is related to the $CH_2$ symmetric bending in cellulose. An additional peak at 1230 $cm^{-1}$, attributed to the C−O stretching vibration of the acetyl group in lignin and hemicellulose, could be observed.[46] The most intense band is located at 1030 $cm^{-1}$, ascribed to the CO and O−H stretching vibration in polysaccharides present in cellulose.[58] Next, the FTIR spectrum of PP-*g*-IA is very similar to that of neat bioPP, which will be commented in the next paragraph. The most remarkable band is located at 1720 $cm^{-1}$, which corresponds to the stretching vibration of the carbonyl groups of IA.[45] DCP exhibits several bands characteristic of a peroxide: C−O−O and C−C−O antisymmetric stretching vibrations at 1265 and 1250 $cm^{-1}$, respectively; symmetric stretching vibration of C−O−O at 1151 $cm^{-1}$; deformation and rocking of $CH_3$ in the isopropyl $-C(CH_3)_2-$ group at 1377, 1358, and 857 $cm^{-1}$; and the presence of monosubstituted benzene rings at 1496, 1445, and 766 $cm^{-1}$.[59]

Referring to the spectra of the bioPP/MPF composites, neat bioPP presents several representative bands. The absorption peaks at 972, 997, and 1165 $cm^{-1}$ are indicative of the $-CH_3$ rocking vibration. At 1375 $cm^{-1}$, the symmetric bending vibration mode of $-CH_3$ is detected.[60] The peak at 2952 $cm^{-1}$ is also ascribed to the methyl group, particularly to its asymmetric stretching vibration.[60] The bands at 1455, 2838, and 2917 $cm^{-1}$ are related to the $-CH_2-$ symmetric bending, $-CH_2-$ symmetric stretching, and $-CH_2-$ asymmetric stretching, respectively.[61] These peaks can be observed in all the composites because bioPP is the base polymer of all the materials developed in this study. The addition of the lignocellulosic MPF filler alters the FTIR spectra, making some additional peaks that have been commented in the individual spectra of MPF to appear. The absorption peak at 3340 $cm^{-1}$ is ascribed to the characteristic O−H stretching vibration and hydrogen bonding in hydroxyl groups, which are present in MPF compounds (cellulose, hemicellulose, pectin, and lignin).[62] The band at 1720 $cm^{-1}$ is indicative of the carbonyl C═O stretching vibration of the linkage of carboxylic


https://doi.org/10.1021/acsapm.2c00373
ACS Appl. Polym. Mater. 2022, 4, 4398−4410

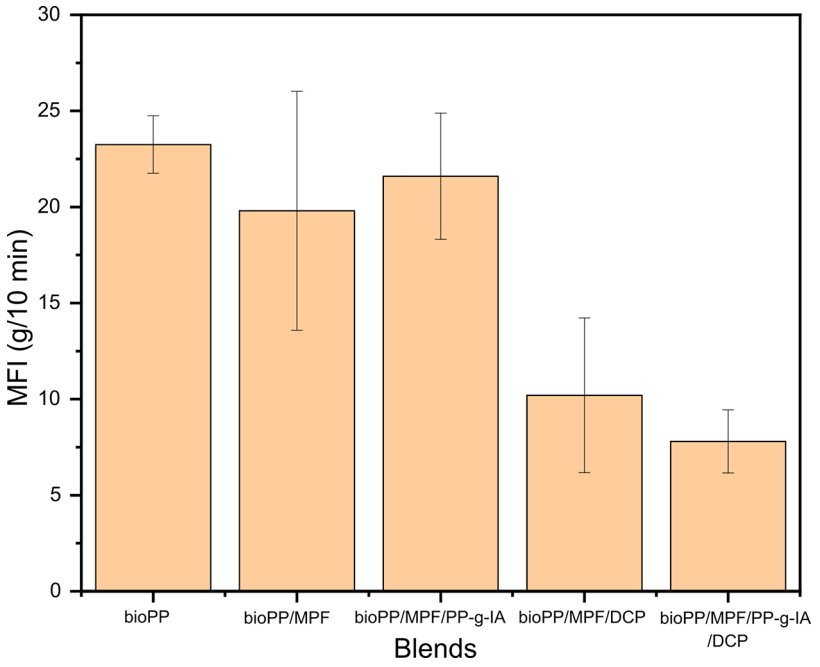


**Figure 5.** MFI of the bioPP/MPF blends at 190 °C/2.16 kg.

acid in lignin or in the ester group in hemicellulose.[63] The little shoulder that is located at 1600 $cm^{-1}$ could be associated with water present in the particles,[64] as they are highly hydrophilic. These bands commented for MPF are also present in all composites containing MPF. The FTIR spectra of the bioPP/MPF/PP-*g*-IA composite does not present any differences in comparison with the uncompatibilized composite. The presence of DCP during extrusion and injection-molding processes did modify the FTIR spectra of the corresponding composites. First of all, at 1263 $cm^{-1}$, an individual peak can be observed ascribed to the asymmetrical stretching of the C−C−O and C−O−O groups present in DCP. Next, another band at 1151 $cm^{-1}$ is seen, related to the symmetric stretching of the C−C−O and C−O−O functionalizations and the stretching of C−O. Finally, an intense peak at 761 $cm^{-1}$ is ascribed to the presence of a monosubstituted benzene ring, which is characteristic of DCP.[59] All these bands have also been observed in the individual FTIR absorption spectrum of DCP. The composite compatibilized by REX with PP-*g*-IA and DCP (bioPP/MPF/PP-*g*-IA/DCP) presents practically all the peaks and bands aforementioned, although the peaks related to the radical-free production of DCP are not so intense in this composite, probably due to certain interactions between PP-*g*-IA and DCP.

**3.8. Effect of the Compatibilization Strategy on the MFI of BioPP/MPF Composites.** Figure 5 shows the MFIs for the different bioPP/MPF composites, measured at 190 °C and a load mass of 2.16 kg. It can be seen that bioPP showed the highest MFI, with a value of 23.25 g/10 min. This value is highly related to a poorly entangled polymer and presents a MFI slightly higher than that reported by Sarabi et al.[65] MPF diminishes the MFI down to 19.8 g/10 min. This is due to the filler proportion in the blend, which influences the rheology of the polymer, substituting the flexible polymer matrix for a more ridged filler, which affects the way polymer chains entangle during the flowing process.[66] Compatibilization with PP-*g*-IA also reduces MFI, which was expected as this compatibilizer improves the interactions between bioPP and MPF, making the entanglement between both compounds and between polymeric chains stronger.[19] As expected, composites obtained by REX with DCP show a drastic reduction of the MFI down to 10.2 g/10 min, which is clearly related to the cross-linking effect of DCP, which improves the bonding between polymeric chains, thus increasing the entanglement of the polymer and making it more rigid and more difficult to flow. Finally, the MFI results of the composite obtained by REX with PP-*g*-IA and DCP again show that the synergistic effect exerted by the combination of the PP-*g*-IA copolymer with DCP during REX improves the entanglement of the polymeric chains, obtaining a more rigid material and thus with lower MFI.

All in all, the results presented here agree with the results observed in the mechanical, thermal, and morphological characterizations, corroborating the compatibilizing efficiency of both PP-*g*-IA and DCP.

## 4. CONCLUSIONS

This work shows the positive effect of the incorporation of MPF in WPCs based on a bioPP matrix with PP-*g*-IA and DCP as compatibilizers. The correct grafting of PP-*g*-IA has also been shown in this study. The addition of this specific load has great potential to be used as a new reinforcement in thermoplastic matrices to make parts by industrial processes, such as injection molding. Regarding mechanical properties, the incorporation of MPF (30 wt %) with PP-*g*-IA exhibited a Young's modulus of 2237 MPa, far superior to the modulus of neat bioPP and bioPP/MPF samples. The addition of DCP to the bioPP/MPF blend further increased this value up to 2280 MPa, and the combined effect of PP-*g*-IA and DCP even increased it further beyond 2349 MPa. This was ascribed to an improvement of the interaction between bioPP and MPF, directly related to the compatibilizing and cross-linking effect of PP-*g*-IA and DCP, respectively. The elongation at break results were quite promising too, going from 15.98% for bioPP/MPF to 29.69% for bioPP/MPF/PP-*g*-IA/DCP. These excellent mechanical properties were corroborated by FESEM


https://doi.org/10.1021/acsapm.2c00373
ACS Appl. Polym. Mater. 2022, 4, 4398−4410

images, which showed a very close gap between the lignocellulosic particles and the polymeric matrix. With regard to thermal properties, the introduction of MPF with compatibilizers leads to an increase in thermal stability and crystallinity, reaching a crystallinity degree of 58% for the sample with PP-*g*-IA, which is another proof of the improvement in mechanical resistance. DMTA results also verified an increase in the stiffness of the materials due to an increase in the storage modulus of the compatibilized samples, confirming the results commented on the mechanical properties, associated with a correct dispersion of the MPF particles in the matrix. Generally, the incorporation of MPF provided the blends with dark brown color that would allow their use in the manufacturing of wood-based products, such as floors, doors, furniture, and so on. Water absorption of the composites also increased as a result of the lignocellulosic nature of the filler. Nonetheless, it was observed how the incorporation of PP-*g*-IA reduced water absorption to a certain degree, which is quite interesting and useful for applications where water absorption is not desirable. Finally, it was also reported on how the compatibilizing and cross-linking effects of PP-*g*-IA and DCP lead to a reduction in the MFI of the composites, directly related to an increase in the adhesion between polymeric chains.

The results obtained in this work indicate the possibility of obtaining biobased WPCs with a considerable natural content of MPF, reducing the cost of the material in relation to the neat bioPP. Moreover, composites with very interesting properties in terms of excellent mechanical properties, in parallel with neat bioPP, enhanced thermal stability, delay in degradation processes, and attractive dark brown color were obtained. All these characteristics make them perfect candidates for substituting wood-based products and make them applicable in several fields. All in all, this work opens a new research route in terms of using MPF as a reinforcing agent and PP-*g*-IA and DCP as successful compatibilizing agents in other composites.

## ■ ASSOCIATED CONTENT

### Supporting Information

The Supporting Information is available free of charge at https://pubs.acs.org/doi/10.1021/acsapm.2c00373.

> Experimental details including FESEM images and histograms of the MPF particles; results, graphics, and analysis including DSC thermograms from the second heating cycle for all the blends; TGA and DTG curves for all the bioPP/MPF blends; plot evolution of the storage modulus and the dynamic damping factor of all the blends supporting the DMTA analysis; water contact angle images of the bioPP/MPF sample; color measurement analysis of all the bioPP/MPF composites; and color coordinates (PDF)

## ■ AUTHOR INFORMATION


### Corresponding Author

**Jaume Gomez-Caturla** − *Technological Institute of Materials (ITM), Universitat Politècnica de València (UPV), 03801 Alcoy, Spain*; orcid.org/0000-0001-8680-4509; Phone: +34 693779697; Email: jaugoca@epsa.upv.es

### Authors

**Rafael Balart** − *Technological Institute of Materials (ITM), Universitat Politècnica de València (UPV), 03801 Alcoy, Spain*

**Juan Ivorra-Martinez** − *Technological Institute of Materials (ITM), Universitat Politècnica de València (UPV), 03801 Alcoy, Spain*; orcid.org/0000-0001-8968-4899

**Daniel Garcia-Garcia** − *Technological Institute of Materials (ITM), Universitat Politècnica de València (UPV), 03801 Alcoy, Spain*

**Franco Dominici** − *Dipartimento di Ingegneria Civile ed Ambientale, University of Perugia, UdR INSTM, 05100 Terni (TR), Italy*

**Debora Puglia** − *Dipartimento di Ingegneria Civile ed Ambientale, University of Perugia, UdR INSTM, 05100 Terni (TR), Italy*; orcid.org/0000-0001-8515-7813

**Luigi Torre** − *Dipartimento di Ingegneria Civile ed Ambientale, University of Perugia, UdR INSTM, 05100 Terni (TR), Italy*

Complete contact information is available at: https://pubs.acs.org/10.1021/acsapm.2c00373


### Author Contributions

The manuscript was written through contributions of all authors. All authors have given approval to the final version of the manuscript. All authors contributed equally.


### Funding

J.G.-C., R.B., J.I.-M., D.G.-G., F.D., D.P., and L.T. received funding from the grant PID2020-116496RB-C22 funded by MCIN/AEI/10.13039/501100011033 (Agencia estatal de Investigación). J.G.-C., R.B., J.I.-M., D.G.-G., F.D., D.P., and L.T. also received funding from Generalitat Valenciana-GVA with grant number AICO/2021/025.


### Notes

The authors declare no competing financial interest.

## ■ ACKNOWLEDGMENTS


J.G.-C. thanks the grant FPU20/01732 funded by MCIN/AEI/10.13039/501100011033 and by ESF Investing in your future. J.I.-M. thanks the FPU19/01759 grant funded by MCIN/AEI/10.13039/501100011033 and by ESF Investing in your future. Microscopy Services at UPV are also acknowledged for their help in collecting and analyzing images.


## ■ REFERENCES


(1) Jorda-Reolid, M.; Gomez-Caturla, J.; Ivorra-Martinez, J.; Stefani, P. M.; Rojas-Lema, S.; Quiles-Carrillo, L. Upgrading Argan Shell Wastes in Wood Plastic Composites with Biobased Polyethylene Matrix and Different Compatibilizers. *Polym* **2021**, *13*, 922.

(2) Xie, S.; Yang, J.; Wang, X.; Yang, J. Synthesis of Fully Biobased Semi-Aromatic Furan Polyamides with High Performance through Facile Green Synthesis Process. *Eur. Polym. J.* **2021**, *162*, 110932.

(3) Torres, F. G.; Rodriguez, S.; Saavedra, A. C. Green Composite Materials from Biopolymers Reinforced with Agroforestry Waste. *J. Polym. Environ.* **2019**, *27*, 2651−2673.

(4) Sakakibara, K.; Moriki, Y.; Tsujii, Y. Preparation of High-Performance Polyethylene Composite Materials Reinforced with Cellulose Nanofiber: Simultaneous Nanofibrillation of Wood Pulp Fibers During Melt-Compounding Using Urea and Diblock Copolymer Dispersant. *ACS Appl. Polym. Mater.* **2018**, *1*, 178−187.

(5) Kalusulingam, R.; Gajula, S.; Koilraj, P.; Shanthana Lakshmi, D.; Tayade, R. J.; Srinivasan, K. Biomass-Derived Humin-Like Furanic Polymers as an Effective Uv-Shielding Agent for Optically Trans-

parent Thin-Film Composites. *ACS Appl. Polym. Mater.* **2021**, *3*, 1932−1942.
(6) Heredia-Guerrero, J. A.; Williams, C. A.; Guidetti, G.; Cataldi, P.; Ceseracciu, L.; Debellis, D.; Athanassiou, A.; Guzman-Puyol, S.; Hamad, W. Y.; Vignolini, S. Plant-Inspired Polyaleuritate−Nanocellulose Composite Photonic Films. *ACS Appl. Polym. Mater.* **2020**, *2*, 1528−1534.
(7) Singha, S.; Gowda, V.; Hedenqvist, M. S. Plant Cuticle-Inspired Polyesters as Promising Green and Sustainable Polymer Materials. *ACS Appl. Polym. Mater.* **2021**, *3*, 4088−4100.
(8) Quiles-Carrillo, L.; Montanes, N.; Garcia-Garcia, D.; Carbonell-Verdu, A.; Balart, R.; Torres-Giner, S. Effect of Different Compatibilizers on Injection-Molded Green Composite Pieces Based on Polylactide Filled with Almond Shell Flour. *Composites, Part B* **2018**, *147*, 76−85.
(9) Schirp, A.; Stender, J. Properties of Extruded Wood-Plastic Composites Based on Refiner Wood Fibres (Tmp Fibres) and Hemp Fibres. *Eur. J. Wood Wood Prod.* **2010**, *68*, 219−231.
(10) Kengkhetkit, N.; Amornsakchai, T. A New Approach to "Greening" Plastic Composites Using Pineapple Leaf Waste for Performance and Cost Effectiveness. *Mater. Des.* **2014**, *55*, 292−299.
(11) Zhou, Y.; Rangari, V.; Mahfuz, H.; Jeelani, S.; Mallick, P. Experimental Study on Thermal and Mechanical Behavior of Polypropylene, Talc/Polypropylene and Polypropylene/Clay Nanocomposites. *Mater. Sci. Eng.* **2005**, *402*, 109−117.
(12) Bahçegül, E. G.; Bahçegül, E.; Özkan, N. 3d Printing of Hemicellulosic Biopolymers Extracted from Lignocellulosic Agricultural Wastes. *ACS Appl. Polym. Mater.* **2020**, *2*, 2622−2632.
(13) Siracusa, V.; Blanco, I. Bio-Polyethylene (Bio-PE), Bio-Polypropylene (Bio-PP) and Bio-Poly(ethylene terephthalate) (Bio-PET): Recent Developments in Bio-Based Polymers Analogous to Petroleum-Derived Ones for Packaging and Engineering Applications. *Polym* **2020**, *12*, 1641.
(14) Avérous, L.; Le Digabel, F. Properties of Biocomposites Based on Lignocellulosic Fillers. *Carbohydr. Polym.* **2006**, *66*, 480−493.
(15) Ouyang, Y.; Mauri, M.; Pourrahimi, A. M.; Östergren, I.; Lund, A.; Gkourmpis, T.; Prieto, O.; Xu, X.; Hagstrand, P.-O.; Müller, C. Recyclable Polyethylene Insulation Via Reactive Compounding with a Maleic Anhydride-Grafted Polypropylene. *ACS Appl. Polym. Mater.* **2020**, *2*, 2389−2396.
(16) Arrakhiz, F. Z.; El Achaby, M.; Kakou, A. C.; Vaudreuil, S.; Benmoussa, K.; Bouhfid, R.; Fassi-Fehri, O.; Qaiss, A. Mechanical Properties of High Density Polyethylene Reinforced with Chemically Modified Coir Fibers: Impact of Chemical Treatments. *Mater. Des.* **2012**, *37*, 379−383.
(17) Zhang, Y.; Chen, J.; Li, H. Functionalization of Polyolefins with Maleic Anhydride in Melt State through Ultrasonic Initiation. *Polym* **2006**, *47*, 4750−4759.
(18) Pesetskii, S. S.; Jurkowski, B.; Makarenko, O. A. Free Radical Grafting of Itaconic Acid and Glycidyl Methacrylate onto Pp Initiated by Organic Peroxides. *J. Appl. Polym. Sci.* **2002**, *86*, 64−72.
(19) Moncada, E.; Quijada, R.; Lieberwirth, I.; Yazdani-Pedram, M. Use of Pp Grafted with Itaconic Acid as a New Compatibilizer for Pp/Clay Nanocomposites. *Macromol. Chem. Phys.* **2006**, *207*, 1376−1386.
(20) Kim, J. S.; Jang, J.-H.; Jeon, D.-G.; Kim, D. H. Preparation of Pp-G-Ia and Its Compatibilizing Effects in Pp/Evoh Blends. *Elastomers Compos.* **2014**, *49*, 225−231.
(21) Rojas-Lema, S.; Ivorra-Martinez, J.; Lascano, D.; Garcia-Garcia, D.; Balart, R. Improved Performance of Environmentally Friendly Blends of Biobased Polyethylene and Kraft Lignin Compatibilized by Reactive Extrusion with Dicumyl Peroxide. *Macromol. Mater. Eng.* **2021**, *306*, 2100196.
(22) Ma, P.; Cai, X.; Zhang, Y.; Wang, S.; Dong, W.; Chen, M.; Lemstra, P. J. In-Situ Compatibilization of Poly(lactic acid) and Poly(butylene adipate-co-terephthalate) Blends by Using Dicumyl Peroxide as a Free-Radical Initiator. *Polym. Degrad. Stab.* **2014**, *102*, 145−151.
(23) Garcia-Garcia, D.; Rayón, E.; Carbonell-Verdu, A.; Lopez-Martinez, J.; Balart, R. Improvement of the Compatibility between Poly (3-Hydroxybutyrate) and Poly (E-Caprolactone) by Reactive Extrusion with Dicumyl Peroxide. *Eur. Polym. J.* **2017**, *86*, 41−57.
(24) Ahmad, E. E. M.; Luyt, A. S. Effects of Organic Peroxide and Polymer Chain Structure on Morphology and Thermal Properties of Sisal Fibre Reinforced Polyethylene Composites. *Composites, Part A* **2012**, *43*, 703−710.
(25) Abdul Aziz, N. A.; Wong, L. M.; Bhat, R.; Cheng, L. H. Evaluation of Processed Green and Ripe Mango Peel and Pulp Flours (Mangifera Indica Var. Chokanan) in Terms of Chemical Composition, Antioxidant Compounds and Functional Properties. *J. Sci. Food Agric.* **2012**, *92*, 557−563.
(26) Safdar, M. N.; Kausar, T.; Nadeem, M. Comparison of Ultrasound and Maceration Techniques for the Extraction of Polyphenols from the Mango Peel. *J. Food Process. Preserv.* **2017**, *41*, No. e13028.
(27) Ferreira, S.; Araujo, T.; Souza, N.; Rodrigues, L.; Lisboa, H. M.; Pasquali, M.; Trindade, G.; Rocha, A. P. Physicochemical, Morphological and Antioxidant Properties of Spray-Dried Mango Kernel Starch. *J. Agric. Food Res.* **2019**, *1*, 100012.
(28) Henrique, M. A.; Silvério, H. A.; Flauzino Neto, W. P.; Pasquini, D. Valorization of an Agro-Industrial Waste, Mango Seed, by the Extraction and Characterization of Its Cellulose Nanocrystals. *J. Environ. Manage.* **2013**, *121*, 202−209.
(29) Pesetskii, S. S.; Jurkowski, B.; Krivoguz, Y. M.; Urbanowicz, R. Itaconic Acid Grafting on Ldpe Blended in Molten State. *J. Appl. Polym. Sci.* **1997**, *65*, 1493−1502.
(30) Shafigullin, L.; Romanova, N.; Gumerov, I.; Gabrakhmanov, A.; Sarimov, D. Thermal Properties of Polypropylene and Polyethylene Blends (Pp/Ldpe). *IOP Conference Series: Materials Science and Engineering*; IOP Publishing, 2018.
(31) Novák, I.; Florián, Š. Study of the Change in Polarity of Polypropylene Modified in Bulk by Polar Copolymers. *J. Mater. Sci.* **2001**, *36*, 4863−4867.
(32) Yadav, S. M.; Yusoh, K. B. Mechanical and Physical Properties of Wood-Plastic Composites Made of Polypropylene, Wood Flour and Nanoclay. *Inter. J. Agric., Forest. Plant.* **2015**, *1*, 52−58.
(33) Poletto, M. Polypropylene-Based Wood-Plastic Composites: Effect of Using a Coupling Agent Derived from a Renewable Resource. *Maderas: Cienc. Tecnol.* **2017**, *19*, 265−272.
(34) Morandim-Giannetti, A. A.; Agnelli, J. A. M.; Lanças, B. Z.; Magnabosco, R.; Casarin, S. A.; Bettini, S. H. P. Lignin as Additive in Polypropylene/Coir Composites: Thermal, Mechanical and Morphological Properties. *Carbohydr. Polym.* **2012**, *87*, 2563−2568.
(35) Joseph, K.; Thomas, S.; Pavithran, C. Effect of Chemical Treatment on the Tensile Properties of Short Sisal Fibre-Reinforced Polyethylene Composites. *Polym* **1996**, *37*, 5139−5149.
(36) Caraschi, J. C.; Leão, A. L. Woodflour as Reinforcement of Polypropylene. *Mater. Res.* **2002**, *5*, 405−409.
(37) Torres-Giner, S.; Montanes, N.; Fombuena, V.; Boronat, T.; Sanchez-Nacher, L. Preparation and Characterization of Compression-Molded Green Composite Sheets Made of Poly(3-Hydroxybutyrate) Reinforced with Long Pita Fibers. *Adv. Polym. Technol.* **2018**, *37*, 1305−1315.
(38) Sari, N. H.; Sanjay, M. R.; Arpitha, G. R.; Pruncu, C. I.; Siengchin, S. Synthesis and Properties of Pandanwangi Fiber Reinforced Polyethylene Composites: Evaluation of Dicumyl Peroxide (Dcp) Effect. *Compos. Commun.* **2019**, *15*, 53−57.
(39) Burgada, F.; Fages, E.; Quiles-Carrillo, L.; Lascano, D.; Ivorra-Martinez, J.; Arrieta, M. P.; Fenollar, O. Upgrading Recycled Polypropylene from Textile Wastes in Wood Plastic Composites with Short Hemp Fiber. *Polymer* **2021**, *13*, 1248.
(40) Naghmouchi, I.; Espinach, F. X.; Mutjé, P.; Boufi, S. Polypropylene Composites Based on Lignocellulosic Fillers: How the Filler Morphology Affects the Composite Properties. *Mater. Des.* **2015**, *65*, 454−461.
(41) Toro, P.; Quijada, R.; Peralta, R.; Yazdani-Pedram, M. Influence of Grafted Polypropylene on the Mechanical Properties of Mineral-Filled Polypropylene Composites. *J. Appl. Polym. Sci.* **2007**, *103*, 2343−2350.


https://doi.org/10.1021/acsapm.2c00373
*ACS Appl. Polym. Mater.* 2022, 4, 4398−4410

(42) Yazdani-Pedram, M.; Menzel, C.; Toro, P.; Quijada, R.; May-Pat, A.; Avilés, F. Mechanical and Thermal Properties of Multiwalled Carbon Nanotube/Polypropylene Composites Using Itaconic Acid as Compatibilizer and Coupling Agent. *Macromol. Res.* **2013**, *21*, 153−160.
(43) Grebowicz, J.; Lau, S. F.; Wunderlich, B. The Thermal Properties of Polypropylene. *Journal of Polymer Science: Polymer Symposia*; Wiley Online Library, 1984; pp 19−37.
(44) Essabir, H.; Bensalah, M. O.; Rodrigue, D.; Bouhfid, R.; Qaiss, A. e. k. Biocomposites Based on Argan Nut Shell and a Polymer Matrix: Effect of Filler Content and Coupling Agent. *Carbohydr. Polym.* **2016**, *143*, 70−83.
(45) Kim, J. S.; Jang, J. H.; Kim, J. H.; Lim, D. Y.; Lee, Y. S.; Chang, Y.-W.; Kim, D. H. Morphological, Thermal, Rheological, and Mechanical Properties of Pp/Evoh Blends Compatibilized with Pp-G-Ia. *Polym. Eng. Sci.* **2016**, *56*, 1240−1247.
(46) Essabir, H.; Hilali, E.; Elgharad, A.; El Minor, H.; Imad, A.; Elamraoui, A.; Al Gaoudi, O. Mechanical and Thermal Properties of Bio-Composites Based on Polypropylene Reinforced with Nut-Shells of Argan Particles. *Mater. Des.* **2013**, *49*, 442−448.
(47) Albano, C.; González, J.; Ichazo, M.; Kaiser, D. Thermal Stability of Blends of Polyolefins and Sisal Fiber. *Polym. Degrad. Stab.* **1999**, *66*, 179−190.
(48) Kim, J. H.; Kim, J. S.; Jang, J. H.; Kim, M. S.; Chang, Y.-W.; Lim, D. Y.; Kim, D. H. Compatibilizing Effects of Polypropylene-*G*-Itaconic Acid on the Polypropylene Composites. *Fibers Polym.* **2016**, *17*, 671−677.
(49) García-García, D.; Carbonell, A.; Samper, M.; García-Sanoguera, D.; Balart, R. Green Composites Based on Polypropylene Matrix and Hydrophobized Spend Coffee Ground (Scg) Powder. *Composites, Part B* **2015**, *78*, 256−265.
(50) Mishra, A. K.; Luyt, A. S. Effect of Sol−Gel Derived Nano-Silica and Organic Peroxide on the Thermal and Mechanical Properties of Low-Density Polyethylene/Wood Flour Composites. *Polym. Degrad. Stab.* **2008**, *93*, 1−8.
(51) Krivoguz, Y. M.; Pesetskii, S. S.; Jurkowski, B.; Tomczyk, T. Structure and Properties of Polypropylene/Low-Density Polyethylene Blends Grafted with Itaconic Acid in the Course of Reactive Extrusion. *J. Appl. Polym. Sci.* **2006**, *102*, 1746−1754.
(52) Vogler, E. A. Structure and Reactivity of Water at Biomaterial Surfaces. *Adv. Colloid Interface Sci.* **1998**, *74*, 69−117.
(53) Noor, S. A. A.; Siti, N. M.; Mahmad, N. J. Chemical Composition, Antioxidant Activity and Functional Properties of Mango (Mangifera Indica L. Var Perlis Sunshine) Peel Flour (Mpf). *Appl. Mech. Mater.* **2015**, *754*−*755*, 1065−1070.
(54) Alonso, D. M.; Granados, M. L.; Mariscal, R.; Douhal, A. Polarity of the Acid Chain of Esters and Transesterification Activity of Acid Catalysts. *J. Catal.* **2009**, *262*, 18−26.
(55) Ichazo, M.; Albano, C.; Gonzalez, J.; Perera, R.; Candal, M. V. Polypropylene/Wood Flour Composites: Treatments and Properties. *Compos. Struct.* **2001**, *54*, 207−214.
(56) George, J.; Bhagawan, S. S.; Thomas, S. Effects of Environment on the Properties of Low-Density Polyethylene Composites Reinforced with Pineapple-Leaf Fibre. *Compos. Sci. Technol.* **1998**, *58*, 1471−1485.
(57) Arrakhiz, F. Z.; El Achaby, M.; Malha, M.; Bensalah, M. O.; Fassi-Fehri, O.; Bouhfid, R.; Benmoussa, K.; Qaiss, A. Mechanical and Thermal Properties of Natural Fibers Reinforced Polymer Composites: Doum/Low Density Polyethylene. *Mater. Des.* **2013**, *43*, 200−205.
(58) Liu, D.; Han, G.; Huang, J.; Zhang, Y. Composition and Structure Study of Natural Nelumbo Nucifera Fiber. *Carbohydr. Polym.* **2009**, *75*, 39−43.
(59) Uhniat, M.; Sudoł, M.; Kudła, S. Stabilisation of LDPE Cross-Linked in the Presence of Peroxidesii. FTIR Study of Chemical Changes Taking Place in the LDPE−Dicumyl Peroxide−Irganox 1081 System. *Polym. Degrad. Stab.* **2000**, *71*, 75−82.
(60) Gopanna, A.; Mandapati, R. N.; Thomas, S. P.; Rajan, K.; Chavali, M. Fourier Transform Infrared Spectroscopy (Ftir), Raman Spectroscopy and Wide-Angle X-Ray Scattering (Waxs) of Polypropylene (Pp)/Cyclic Olefin Copolymer (Coc) Blends for Qualitative and Quantitative Analysis. *Polym. Bull.* **2019**, *76*, 4259−4274.
(61) Larkin, P. *Infrared and Raman Spectroscopy: Principles and Spectral Interpretation*; Elsevier, 2017.
(62) Spinacé, M. A. S.; Lambert, C. S.; Fermoselli, K. K. G.; De Paoli, M.-A. Characterization of Lignocellulosic Curaua Fibres. *Carbohydr. Polym.* **2009**, *77*, 47−53.
(63) Olsson, A.-M.; Salmén, L. The Association of Water to Cellulose and Hemicellulose in Paper Examined by Ftir Spectroscopy. *Carbohydr. Res.* **2004**, *339*, 813−818.
(64) Paiva, M.; Ammar, I.; Campos, A.; Cheikh, R.; Cunha, A. Alfa Fibres: Mechanical, Morphological and Interfacial Characterization. *Compos. Sci. Technol.* **2007**, *67*, 1132−1138.
(65) Sarabi, M. T.; Behravesh, A. H.; Shahi, P.; Daryabari, Y. Effect of Polymeric Matrix Melt Flow Index in Reprocessing Extruded Wood−Plastic Composites. *J. Thermoplast. Compos. Mater.* **2014**, *27*, 881−894.
(66) Ariff, Z. M.; Ariffin, A.; Jikan, S. S.; Rahim, N. A. A. Rheological Behaviour of Polypropylene through Extrusion and Capillary Rheometry. *Polypropylene*; InTech, 2012; pp 29−49.





https://doi.org/10.1021/acsapm.2c00373
*ACS Appl. Polym. Mater.* 2022, 4, 4398−4410